Cellulose (2021) 28:3311–3325
https://doi.org/10.1007/s10570-021-03765-2

ORIGINAL RESEARCH

Insights into the microstructures and reinforcement mechanism of nano-fibrillated cellulose/MXene based electromagnetic interference shielding film

Xuran Xu · Shuaining Wu · Jian Cui · Luyu Yang · Dingyao Liu · Yongzheng Zhang · Xiao Chen · Kai Wu · Dongping Sun

Received: 9 November 2020 / Accepted: 6 February 2021 / Published online: 20 February 2021

Abstract Recently, with the high requirement of electromagnetic interference (EMI) shielding materials, micro- or nano-fibrillated cellulose reinforced $Ti_3C_2T_x$ nanosheets (transition-metal carbides/carbonitrides, MXene) composites have attracted wide attention due to their complementary functional properties. Nevertheless, it is still challenging to overcome a trade-off between EMI shielding performance and mechanical enhancement with the addition of reinforcing fillers. Herein, modified bacterial cellulose nanofiber (BCNF), with well-tuned micro structure, is employed as the unique reinforcing unit to self-assembly with MXene. The mechanical and electrical properties of different cellulose-derived composites were further compared to get insights into the effect of the fiber configuration on reinforcing properties. Particularly, the optimized MXene/BCNF sample simultaneously exhibited high tensile strength (252.2 MPa), excellent folding endurance (> 10,000 times), and high electrical conductivity (443.5 S cm^{-1}). With striking shielding effectiveness (19,652 dB cm^2 g^{-1}), the sample effectively interferes with emitted electromagnetic waves, and is therefore a promising candidate for wearable devices and human electronic equipment.

Xuran Xu, Shuaining Wu have contributed equally to this work.

Supplementary Information The online version contains supplementary material available at https://doi.org/10.1007/s10570-021-03765-2.

X. Xu · S. Wu · J. Cui · L. Yang · Y. Zhang · X. Chen (✉) · D. Sun (✉)
Institute of Chemicobiology and Functional Materials, School of Chemical Engineering, Nanjing University of Science and Technology, 200 Xiao Ling Wei, Nanjing 210094, People's Republic of China
e-mail: chen_xiao5715@163.com

D. Sun
e-mail: sundpe301@163.com

D. Liu · K. Wu (✉)
College of Polymer Science and Engineering, State Key Laboratory of Polymer Materials Engineering, Sichuan University, Chengdu 610065, People's Republic of China
e-mail: kaiwuscu@163.com

Graphic abstract

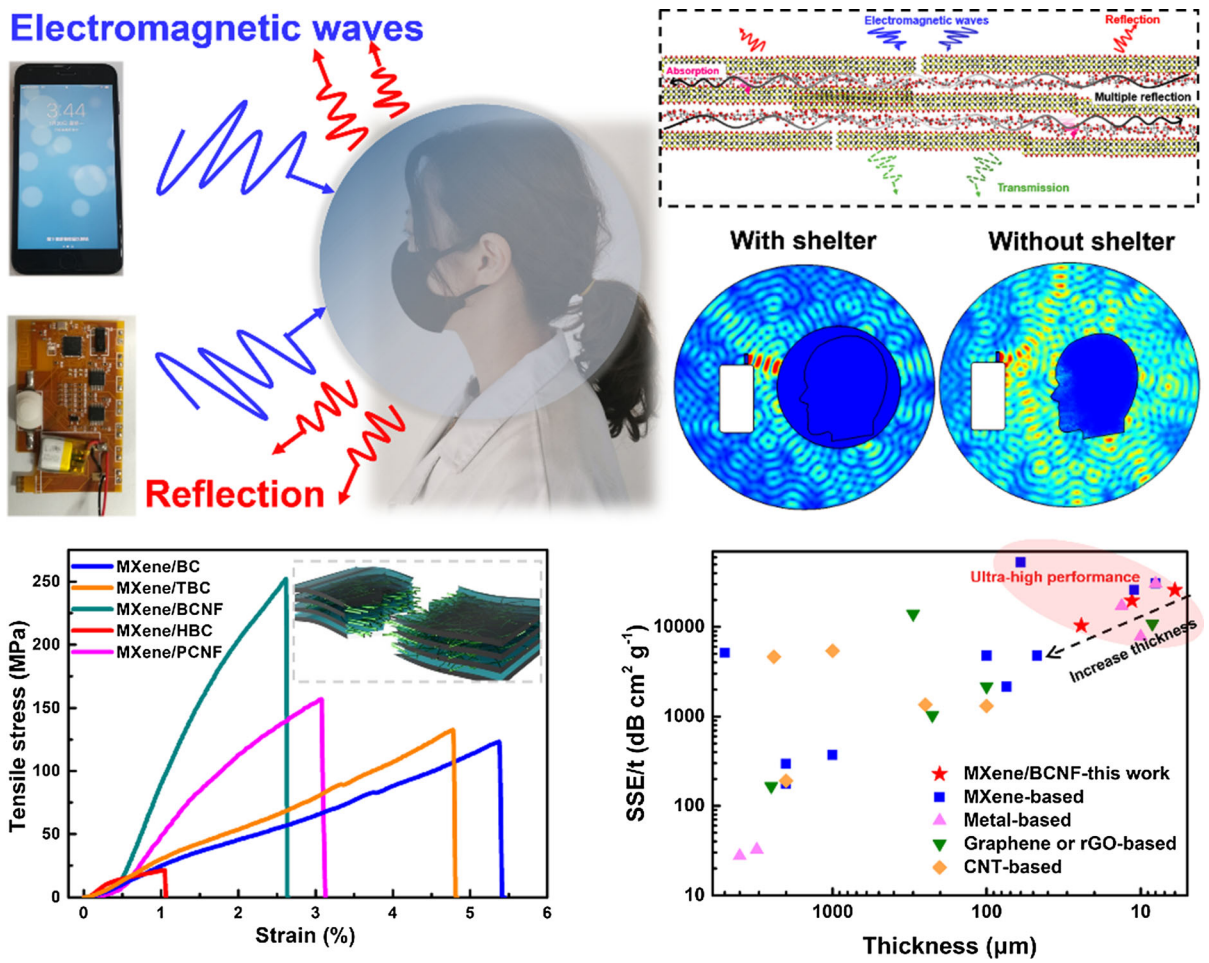

Keywords Mxene · Cellulose nanofiber · Electromagnetic interference shielding · Mechanical property

Introduction

With the rapid popularity of portable communication equipment and wearable electronics, electromagnetic radiation has emerged as a serious problem due to its potential detrimental effects on human health and signal propagation (Sage and Burgio 2018; Yadav et al. 2018; Zhang et al. 2018). Electromagnetic interference (EMI) shielding materials, with light weight, good flexibility and high shielding efficiency, are highly required as the effective shelter for relieving the electromagnetic radiation from these wearable resources (Shen et al. 2014; Yan et al. 2015; Yu et al. 2018). Metal materials are considered as a traditional choice, while their promotion and widespread application are largely restricted by the drawbacks of high weight, poor flexibility and easy corrosion (Lee et al. 2017; Wan et al. 2018). Recently, 2D carbon-based nanomaterials (Joseph et al. 2017; Liang et al. 2019; Zeng et al. 2017; Zhao et al. 2018), typically transition-metal carbides/carbonitrides [i.e. $Ti_3C_2T_x$ (MXene)], have attracted expanded attention in EMI shielding (Cao et al. 2019a; Wang et al. 2019a, 2019b; Zhang et al. 2019) due to the remarkable electrical

conductivity (Geng et al. 2019; Xiong et al. 2018) and high dielectric loss as well as non-toxicity (Liu et al. 2017; Valekar et al. 2017; Zeng et al. 2016). However, their weak interplanar van der Waals interactions between overlapped MXene planes usually result in a weak-assembled macrostructure, thus leading to the low mechanical strength of neat papery film (Kumar 2019; Ma et al. 2020). Therefore, efforts have been made to achieve a percolated reinforcing skeleton using large aspect ratio fillers (Tang et al. 2019) to satisfy the mechanical requirements in practical applications (Cao et al. 2019b; Liu et al. 2018, 2019; Ma et al. 2020; Weng et al. 2018; Xie et al. 2019b).

Utilization of 1D polymer nanofiber as the reinforcing component (Palazzetti and Zucchelli 2017; Xie et al. 2019a), for example cellulose nanofiber (CNF), has proved to be one of the most efficient strategy for constructing the stable layer-by-layer self-stacking 2D MXene/1D CNF macrostructure (Ma et al. 2021; Rahman et al. 2019; Tian et al. 2019). Compared with other polymer fillers, cellulose nanofiber could greatly reduce the contact resistance between overlapped MXene planes, thus enhancing the mechanical properties while maintaining the high electrical conductivity (Chen et al. 2020; Wang et al. 2020). For example, a nacre-like MXene/CNF composite film with an EMI SSE of 2647 dB cm^2 g^{-1} was fabricated by a facile vacuum-filtration self-assembly method, in which percolated 1D CNF network could both strengthen and toughen the composite film (135.4 MPa) due to the unique nacre-like lamellar structure and strong MXene-CNF interfacial interactions (Cao et al. 2018). Another work reported a MXene/CNF composite film with an alternating multilayered structure, in which tightly packed CNF layers could prevent the zigzag cracks in MXene layers, thus resulting in an improved mechanical strength (112.5 MPa) with excellent EMI SSE (7029 dB cm^2 g^{-1}) at the thickness of only 35 μm (Zhou et al. 2020). However, it should be noted that an inevitable decrease in EMI SSE of MXene/CNF composite film is still accompanied with the enhancement in tensile strength by the addition of reinforcing CNF. The optimization between the percolated reinforcing CNF network and CNF-MXene contact resistance remains challenges (Malucelli et al. 2019; Nie et al. 2020). Therefore, ideal configurations such as higher-aspect, better dispersion, and stronger inter-fiber interactions are highly expected for cellulose fillers in order to the provide extraordinary mechanical properties together with well-preserved EMI shielding performance for practical applications.

In this study, modified bacterial cellulose nanofiber (BCNF) with a typical interconnected conformation and an ultrathin thickness (30–50 nm) (Gao et al. 2019; Wang et al. 2017), has been used as a reinforcing substrate to prepare MXene-based EMI shielding film. Different from widely reported CNF, its high aspect ratio could provide less contact resistance and the strong inter-fiber connections could act as an effective mechanically enhanced interlock (Hua and Fei 2019). Therefore, a tightly packed 2D/1D lamellar structure was built with well-percolated BCNF reinforcing skeleton and continuous MXene-MXene conductive paths. A comparative study on the mechanical and electrical properties of different cellulose-derived composite films were further evaluated to get insights into the reinforcing mechanism. As a result, at an extremely low thickness of only 11.4 μm, the MXene/BCNF sample exhibited a high tensile strength (252.2 MPa), excellent flexibility (folding endurance more than 10,000 times) as well as high EMI SSE (19,651 dB cm^2 g^{-1}), outperforming most reported MXene-based paper-like films. With the excellent comprehensive mechanical and EMI shielding performances, the MXene/BCNF composite film presents potential applications in preventing human from continuous interference by electromagnetic waves.

Experimental

Materials and characterizations

All the reagents and characterizations used in this study are described in Supporting Information (SI).

Fabrication of cellulose-derived nanofibers

Raw BC were cultivated using an *Acetobacter xylinum* NUST4.2 through a dynamic fermentation process at 30 °C as reported previously (Yan et al. 2017). After the fermentation, the sample was treated with 0.1% sodium hydroxide solution and hydrogen peroxide at 80 °C for 6 h to remove the bacteria and finally washed with distilled water several times. The dispersed BCNF was prepared by a TEMPO oxidation followed with a high-pressure treatment. Typically,

2.0 g prefabricated BC was dispersed in 200 mL PBS buffer (0.05 M, pH 6.8) and stirred at 60 °C for 30 min in a sealed flask. Then TEMPO (0.036 g, 0.2 mmol) was added and stirred. After this, $NaClO_2$ (3 mmol) and NaClO (30 mmol) were added into the suspension and stirred at 60 °C for 24 h. The TEMPO oxidation was quenched by adding 10 mL ethanol, and the TEMPO-oxidized BC was obtained after washing, centrifugation for several times. Finally, the diluted products (0.5 wt%) were homogenized in a high-pressure homogenizer (AH-2010, ATS Engineering Inc., Canada) at pressure levels of 100 MPa and for up to 30 HPH cycles. The raw CNF with only high-pressure treatment (PCNF) and acid hydrolyzed BC nanofiber (HBC) were also prepared for comparison (Yan et al. 2017).

Fabrication of delaminated $Ti_3C_2T_x$ nanosheets

The delaminated $Ti_3C_2T_x$ nanosheets were obtained by selectively etching the Al from Ti_3AlC_2 (Zhang et al. 2017). Typically, 1.0 g Ti_3AlC_2 was added in 20 mL, 6 M HCl containing 1.0 g LiF under magnetic stirring at 35 °C for 24 h. The resulting suspension was washed with distilled water and centrifuged at 6000 rpm several times to obtain the clay-like Ti_3C_2-Tx sediment. Subsequently, the sediment was dispersed in deionized water and ultrasonicated for 3 h to obtain delaminated Ti_3C_2 nanosheets, named as MXene. The MXene samples were then collected by a centrifugation process and freeze-dried for 24 h. Finally, 0.5 wt% MXene suspension was prepared for the following experiment.

Fabrication of MXene/BCNF composite films

The $Ti_3C_2T_x$ nanosheets and BCNF suspension with a total weight of 6.0 g were dispersed in 50 mL deionized water under ultrasonication for 5 min. A series of MXene/BCNF-x composite films was obtained by the vacuum filtration and dried under ambient temperature. The value of x represents the weight percentage of MXene. Afterwards, the films with different thickness were prepared with a total suspension weight of 3.0 g, 6.0 g, 9.0 g, 12.0 g and 15.0, respectively. Meanwhile, the MXene/other cellulose-derived composite films were prepared as control groups under the same conditions.

Results and discussions

Morphology and macrostructures

The most intriguing design of this study is the combination of 2D MXene with the well-tuned BCNF to guarantee the good conjunction between the electromagnetic interference (EMI) shielding performance and mechanical enhancement as shown in Fig. 1a. Herein, BC, with the typical 3D interconnected conformation, was cultivated through a dynamic fermentation process as shown in Fig. S1a (Krasteva et al. 2017; Tian et al. 2019). Although the strong inter-fiber interactions contribute to effective mechanical enhancements (Huang et al. 2019), they may also induce obvious aggregations during vacuum-assisted filtration, resulting in contact resistance reducing and tight MXene-BC stacking. Therefore, a gentle TEMPO-oxidation treatment followed with high-pressure homogenization was carried out. AFM image in Fig. S1b manifests that the obtained BCNF preserves a well-tuned conformation with an ultrathin thickness of only 30–50 nm, which is expected to be beneficial for mechanical enhancement and the reduction of MXene-MXene contact resistance. MXene was synthesized by selective etching Ti_3AlC_2 (MAX, Fig. S2) in a mixture of HCl and LiF, and the etched powder was delaminated by manual shaking to form a stabilized dispersion. From the morphology characterization in Fig. 1b and c, one can see that the delaminated MXene nanosheets presents large dimension with a thickness of only 4.23 nm. The final MXene/BCNF composite film could also exhibit excellent flexibility and foldability as shown in Fig. 1d.

To get insights into the effect of cellulose configurations on the microstructure of the composites, we first characterized the morphology of different cellulose-derived composite films including MXene/BC, MXene/BCNF, MXene/HBC, and MXene/PCNF. As the TEM images shown, compared with pure BC (Fig. 2a), HBC (Fig. 2e) and PCNF (Fig. 2g), the BCNF presented best dispersion and highest aspect ratio with fiber diameter of 20–30 nm (Fig. 2c). The particle size distributions of different fibers were also investigated as shown in Fig.S3, one can see that the HBC and BCNF present smaller size distributions compared to BC and PCNF, which are consistent with structural characterization. As shown in Fig. 2d and

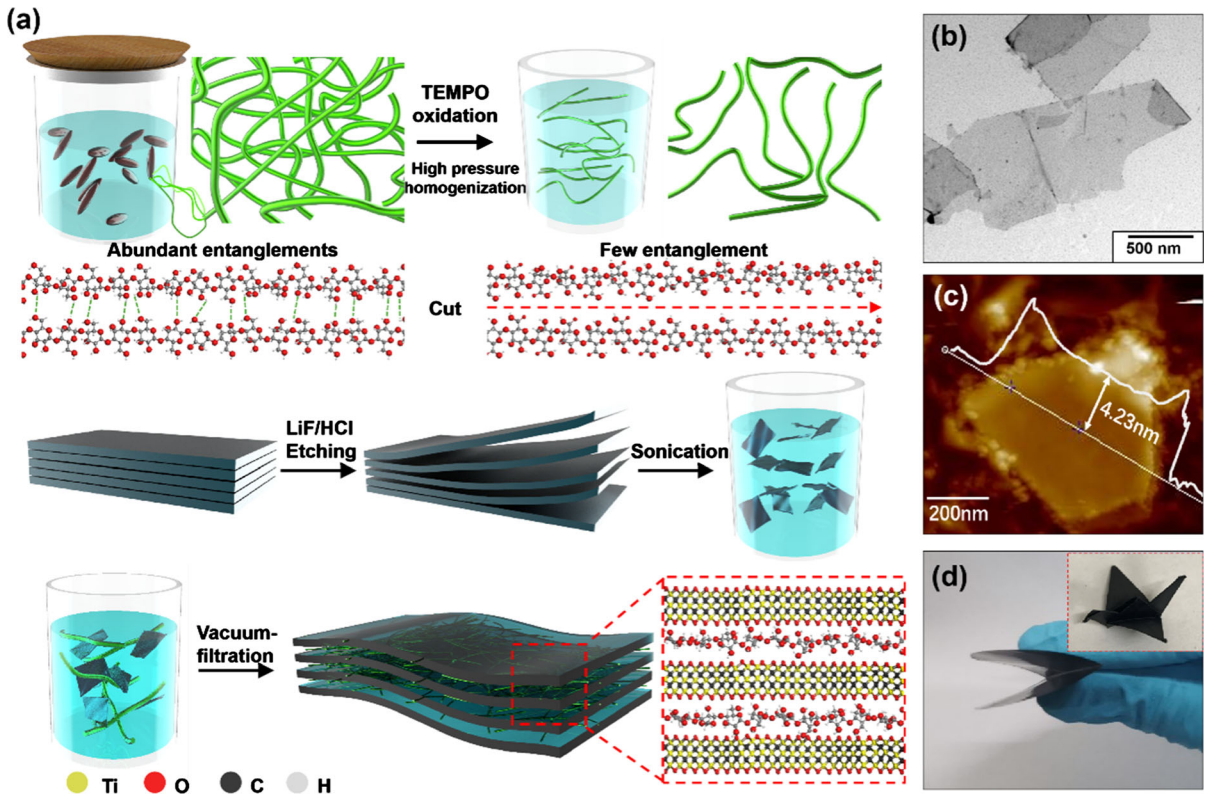

Fig. 1 **a** Schematic illustration of the fabrication process of the MXene/BCNF composite film; **b** TEM and **c** AFM micrographs of MXene; **d** digital image of a folded MXene/BCNF composite film and a small paper crane prepared by folding the composite film

Fig. S4, the porous layered structure of the pure MXene film could be gradually transformed into a tightly stacked, orderly layer-by-layer and nacre-like counterpart in MXene/BCNF composite film. The tightly stacked and dense 2D/1D structure is finally confirmed by AFM image in Fig. S5, which possesses a relatively smooth surface without obvious local folds, defects or fractures in the composite film. In comparison, due to a large number of inter-fiber entanglements and connections, the MXene sheets are arranged in an inclined way along the base direction in both MXene/BC and MXene/HBC samples (Fig. 2b, f), which may prevent the effective orientation and tight inter-layer self-assembly, resulting in crimp or stack between layers. Even though a more ordered microstructure can be obtained for MXene/PCNF composite film as shown in Fig. 2h, there still exists some random defects because of the strong interaction between fibers. Therefore, with a well in-plane orientated and tightly stacked microscopic lamellar structure, the MXene/BCNF composite film is expected to provide excellent mechanical properties and electrical properties in the following tests.

The successful TEMPO-oxidation of BCNF may be deduced from the FT-IR spectra in Fig. 3a. In the pure BC spectra, the peak in 3347 cm^{-1} is attributed to the tensile vibrations of hydroxyl and the peak groups at 1290 cm^{-1} are related to the tensile vibrations of C–H carbohydrates. The 1159 cm^{-1} peak corresponds to the asymmetric tensile bonding of the C–O. The peak at 1050 cm^{-1} is attributed to hydroxyl and C–O–C groups and tensile vibrations of carbohydrates. The characteristic peak at 1598 cm^{-1} corresponding to C=O stretching of –COOH is observed in the spectrum of TEMPO-oxidized bacterial cellulose. This typical treatment is considered to be beneficial for not only the remove of the amorphous counterpart, but also the weakness of the inter-fiber hydrogen-bonding interactions while preserving some inter-fiber crystalline connections (Luo et al. 2013). The crystalline structures of the MXene/BCNF products were also characterized by XRD with patterns shown in Fig. 3d. One

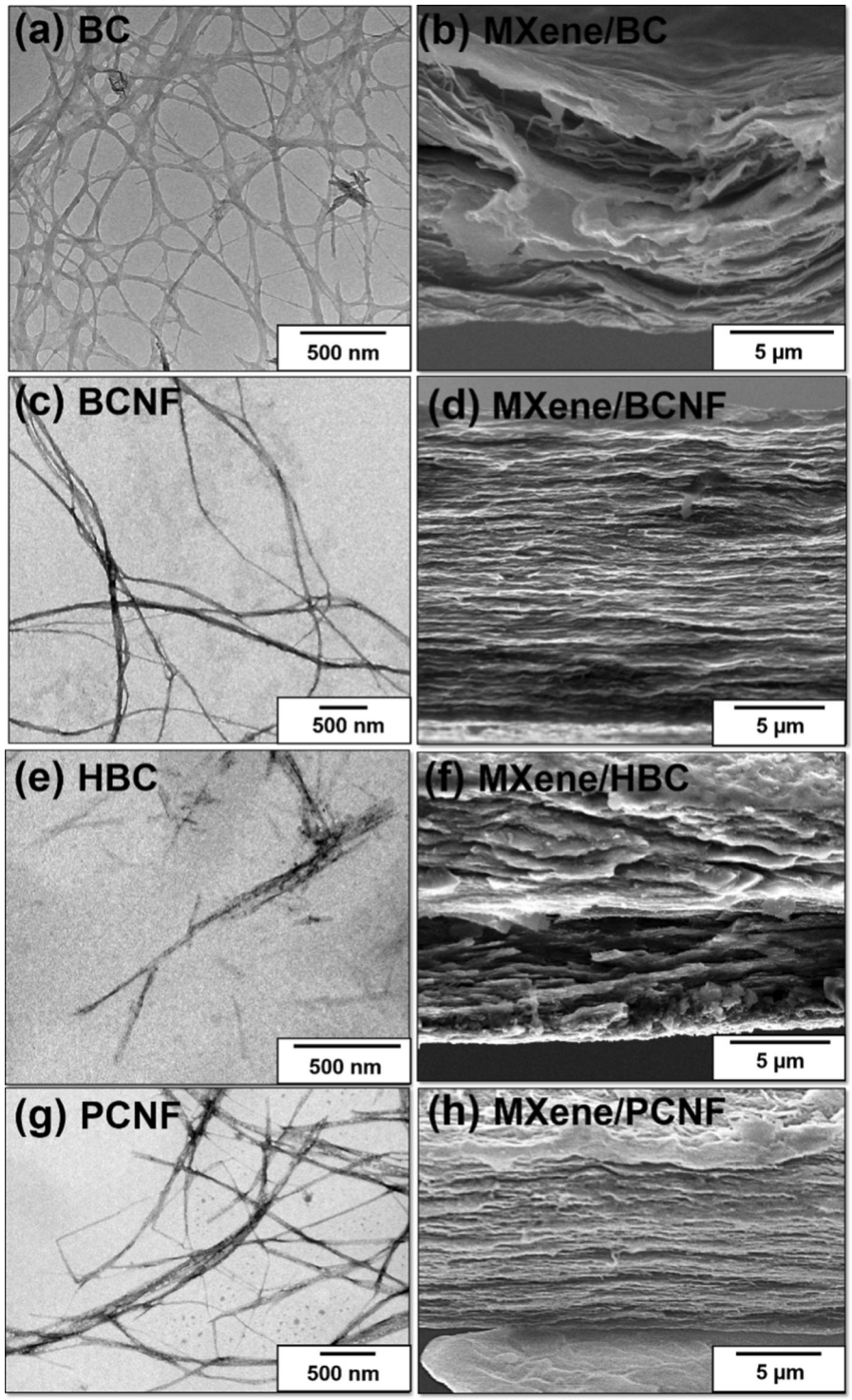

Fig. 2 TEM micrographs of **a** pure BC, **c** BCNF, **e** HCF, **g** PCNF; Cross-section SEM images of **b** MXene/BC, **d** MXene/BCNF, **f** MXene/HCF, and **h** MXene/PCNF

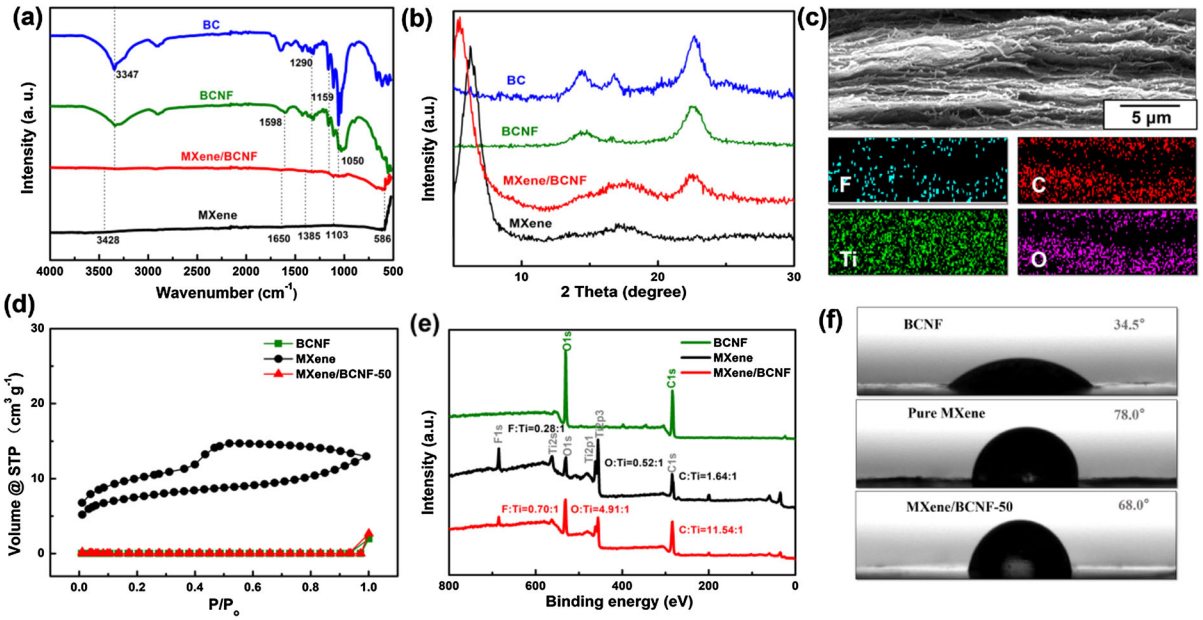

Fig. 3 **a** FT-IR spectra, **b** XRD analysis of pure BC, BCNF, pure MXene and MXene/BCNF-50; **c** Cross-section SEM image and elemental mapping of the tensile-fracture MXene/BCNF-50 composite film; **d** BET specific surface areas, **e** XPS spectra and **f** Water contact of BCNF, MXene and MXene/BCNF-50

can see the typical peaks of the cellulose I at 14.8°, 16.7° and 22.3° in all BC-based samples, corresponding to the (101), (10$\bar{1}$) and (002) crystal planes (Wang et al. 2018). Moreover, in the MXene/BCNF film, the characteristic peak of MXene shifts from 2θ = 6.2° to 5.5°, implying that the percolated reinforcing network of interconnected BCNF are successfully intercalated into the overlapped MXene nanosheets to form the homogeneously assembled lamellar structure (Song et al. 2020). EDS mapping image of the cross-section by a rapid stretching in Fig. 3c demonstrates that MXene could form continuous conductive paths in the in-plane direction. This could also be deduced from the BET results in Fig. 3d, in which BET specific surface areas of 24 m^2 g^{-1} for pristine MXene film has decreased to almost zero for MXene/BCNF film, signifying the typical importance of BCNF's configuration. We further investigated the chemical compositions and element status of MXene/BCNF samples by XPS measurement. Figure 3e shows that the pure MXene has the F/Ti atomic ratio of 0.28, O/Ti atomic ratio of 0.52, C/Ti atomic ratio of 1.64. After the introduction of BCNF, three of the above atomic ratios increase to 0.70, 4.91 and 11.54. The surface hydrophilicity of the samples was finally characterized by water contact angle measurements. Figure 3f shows that the introduction of BCNF effectively improves the hydrophilicity of the composite film, thus improving its human skin affinity for the wearable applications.

Mechanical properties

A comparative study of the mechanical properties between MXene/BCNF composite film and other cellulose-derived composite films is first conducted under the same MXene weight fraction. As shown in Fig. 4a, MXene/BCNF composite film presents the highest tensile strength and outperforming toughness among these four types of cellulose-based composites films, signifying the critical role of the ultrafine but interconnected configuration of BCNF. To further explore the effect of cellulose content on mechanical properties, pure MXene, BCNF and MXene/BCNF-12.5 to 87.5 films were compared by tensile strain test as shown in Fig. 4b–f. Pure MXene exhibits the lowest tensile strength and fracture strain (33.9 ± 7.2 MPa, 1.4 ± 0.2%), probably due to the weak interplanar interactions and obvious inner hole defects. However, these values are greatly improved after introducing the interconnected BCNF. For example, the tensile strength of the composite film is improved to

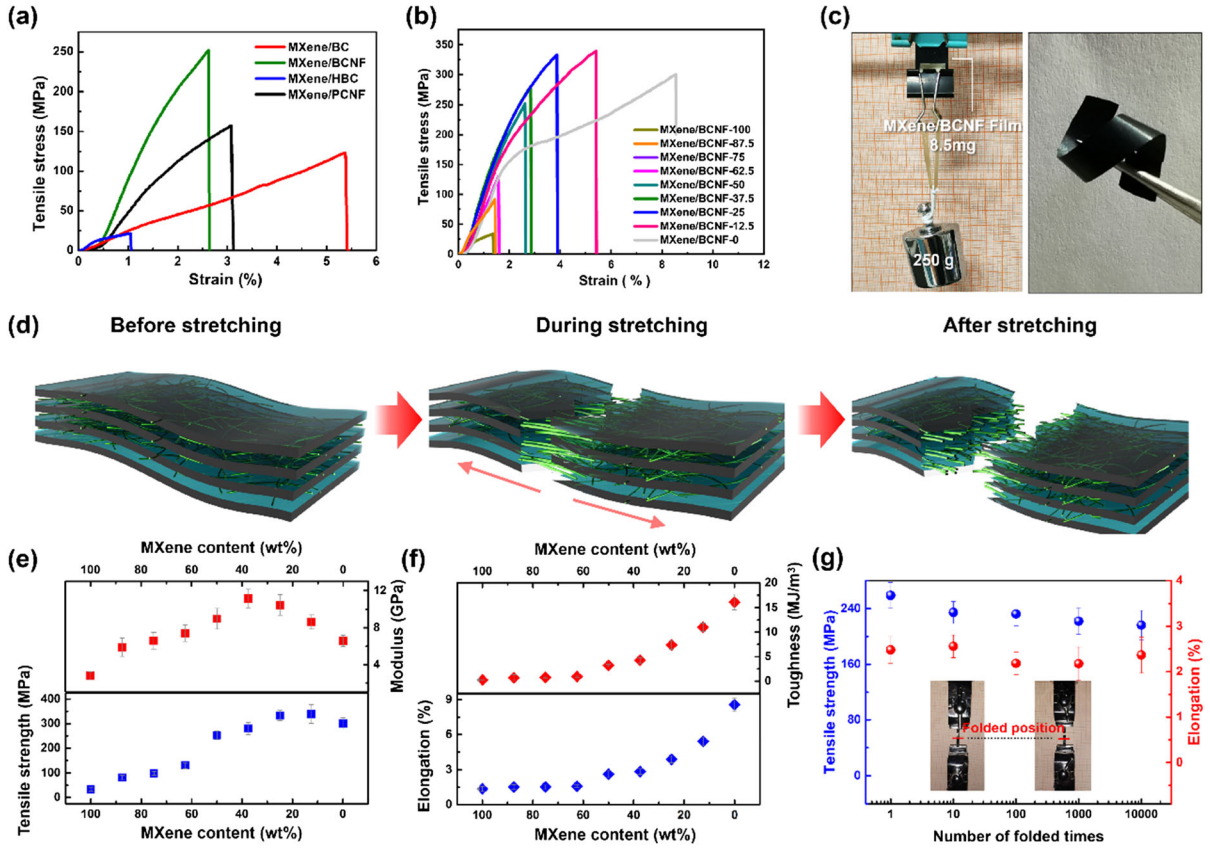

Fig. 4 **a** Tensile stress–strain curves of MXene/BC-50, MXene/BCNF-50, MXene/HBC-50 and MXene/PCNF-50 composite films; **b** tensile stress–strain curves of pure BCNF film, pure MXene film and MXene/BCNF-12.5 to 87.5 composite films; **c** digital images of the MXene/BCNF-50 composite film that can withstand a weight of 250 g, and show a super-flexibility; **d** schematic of stretching process of MXene/BCNF composite films; **e** tensile strength and modulus and **f** elongation and toughness of MXene/BCNF-0 to 100 composite films; **g** tensile strength and elongation of folded MXene/BCNF-50 composite film

81.5 ± 9.2 MPa (2.5 times higher than pure MXene film) with the loading rate of only 12.5% BCNF. The optimized tensile strength (> 250 MPa) is achieved at the weight fraction of MXene from 0 to 62.5%, where MXene/BCNF composite films perform the both tightly packed macrostructure and well-percolated reinforcing BCNF network. It is also known that over loading of BCNF may reduce the electrical conductivity so that prevent EMI shielding efficiency. Therefore, 50% BCNF loading is taken as the optimal condition and the main object for the subsequent EMI performance tests. At this critical content, MXene/BCNF composite film exhibits excellent comprehensive mechanical properties with Young's modulus, elongation and toughness achieving to 9.0 GPa, 2.6% and 3.2 MJ/m^3, respectively. The possible stretching process of MXene/BCNF composite films is illustrated in Fig. 4d. The robustness of MXene/BCNF composite film is attributed to the effective enhancement effect of well-percolated and interconnected BCNF, which could serve as the interlocks to dissipate the tensile stress. During the stretching process, MXene plates are broken into zigzag shape, while BCNF could be further straightened and slippage to enable a large elongation, which is also beneficial to the toughness of MXene/BCNF composite film.

To further investigate the folding endurance of the MXene/BCNF composite film, the MXene/BCNF-50 film was chosen to be folded by a 100 g weight for 1 to 10,000 times. As shown in Fig. 4g, after 10,000 times of folding, the tensile strength and elongation of the composite film could be well-preserved to

216.3 ± 21.1 MPa and 2.37 ± 0.39%, respectively. Meanwhile, the fracture location showed slightly change after 10,000 folds, indicating that the remarkable folding endurance. Furthermore, digital images in Fig. 4c show that this composite film could withstand a 250 g weight that is almost 30,000 times of its own weight, and it could also be repeatedly bended and folded without any rupture, which is also a significant proof of concept for its high strong and flexible performances.

Electrical conductivity and EMI shielding performance

Generally, the intrinsic electrical conductivity of flexible composite film is one of the most critical factors for its EMI shielding performance. In our work, due to the well-tuned micro structure of BCNF, the design of nacre-like architectures of MXene/BCNF films is believed to be beneficial to maintain the continuous morphology from the single-layer perspective. This architecture would also provide more low-defects and high-efficiency electron pathways, leading to higher electrical conductivity and better EMI performances (Fang et al. 2015; He et al. 2019b). Firstly, we compared the electrical conductivity of different cellulose-derived composite films as shown in Fig. S6. One can see at the high BCNF loading of 50 wt%, MXene/BCNF film could still maintain the high electrical conductivity of 443.5 ± 83.0 S cm^{-1} (Fig. 5a). We deduced that with high-aspect ratio, ultrathin thickness and interconnected configuration, BCNF could relieve most contact resistance between MXene-MXene overlaps, resulting in superior electrical conductivity among different cellulose derived MXene films. This high electrical conductivity is responsible for the corresponding excellent EMI SE (Fig. 5b). The MXene/BCNF-50 composite film could maintain the high value of 41.2 dB at the frequency ranging from 8.2 to 12.4 GHz (X-band), which is comparable to that of pure MXene film (52 dB).

To further explore the EMI shielding mechanism of the MXene/BCNF composite film, the total EMI SE (SE_T), EMI absorption efficiency (SE_A) and EMI reflection efficiency (SE_R) at the frequency of 12.4 GHz are calculated (Supporting Information) and presented in Fig. 5c. As can be seen, when the MXene content is less than or equal to 25 wt%, the SE_A value is lower than SE_R, reflecting that the shielding performance of the composite film is mainly due to reflection. However, when the MXene content is more than 37.5 wt%, the SE_A makes more contribution to the shielding efficiency than SE_R. At this condition, the value of SE_A/SE_T is stable at above 60%. This is ascribed to the unique 2D/1D lamellar structure that allows electromagnetic waves to be multiply absorbed and reflected between the continuously MXene-MXene conductive pathways. However, when the continuous MXene paths are destroyed, the SE_A caused by multiple absorption and reflection will decline significantly. Generally, in comparison with SE_R, SE_A is more welcome as it could gainfully prevent the secondary electromagnetic radiative pollution. Based on above considerations, the MXene/BCNF-50 composite film, with the most outstanding EMI shielding performance and optimal mechanical properties, was chosen as optimized sample for the following studies. With increasing the thickness of MXene/BCNF composite film from 6.0 to 11.4 μm, the EMI SE increases obviously in whole X-band (Fig. 5d), while after 11.4 μm, the increasing trend performs negatively. In addition, as increase of the thickness, SSE/t that describes the specific shielding efficiency also decreases from 25,851 to 8974 dB cm^2 g^{-1} (Fig. S7). It suggests that at the high thickness, MXene's in-plane orientation may be hindered and some hole defects or aggregations may be inevitable during the vacuum-filtration induced 2D/1D self-assembly process. Therefore, MXene/BCNF composite film with the thickness of 11.4 μm is the optimized one, which is then chosen as the research sample and has been folded for different times to explore the folding durance. Interestingly, both EMI SE and SSE/t perform a stable trend, even though a 100 g weight oppressed folding process has been carried for 10,000 times to this MXene/BCNF composite film, demonstrating its excellent flexibility and durable EMI shielding capability. We also compare this composite film with most of the metal-based and carbon-based EMI shielding materials (Fig. 5f and Table S1), our MXene/BCNF-50 composite films with different thickness (i.e. 6.0, 11.4 and 24.3 μm) behave the outstanding SSE/t values (10,355 ∼ 25,851 dB cm^2 g^{-1}) and great mechanical strength among the MXene-based composite films, which are almost equal to the values of pure MXene (25,863 dB cm^2 g^{-1}) (Shahzad et al. 2016), pure graphene (10,822 dB cm^2 g^{-1}) (Shen et al. 2014), and metal

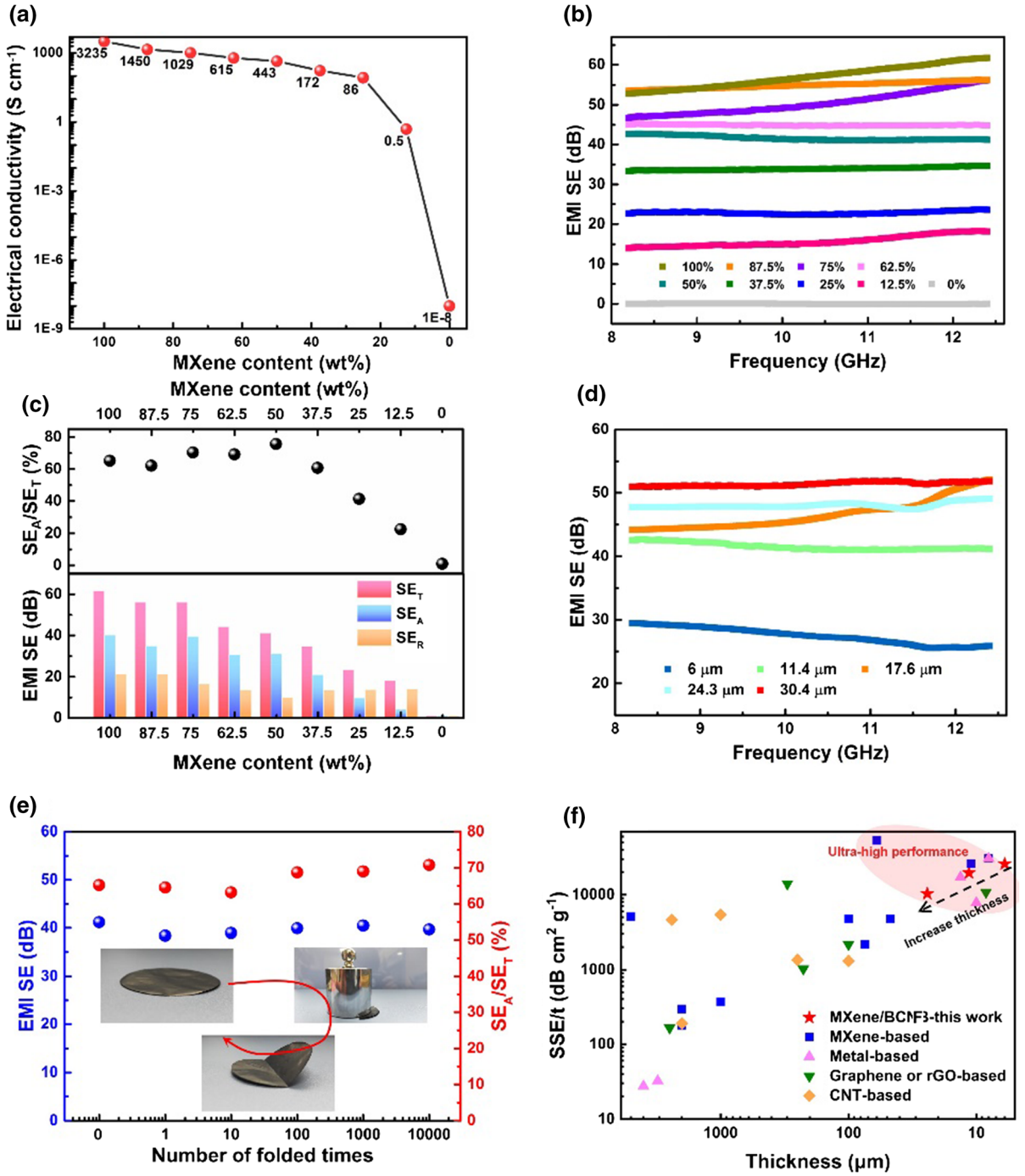

Fig. 5 **a** Electrical conductivity, **b** EMI shielding performance at whole X-band, **c** total EMI SE (SE_T), EMI absorption efficiency (SE_A), EMI reflection efficiency (SE_R) and SE_A/SE_T values at the frequency of 12.4 GHz of MXene/BCNF composites film; **d** EMI shielding performance of MXene/BCNF-50 composite films with different thicknesses at whole X-band; **e** EMI SE and SE_A/SE_T values of folded MXene/BCNF-50 composite films; **f** Comparison of SSE/t value as a function of thickness with previous reports

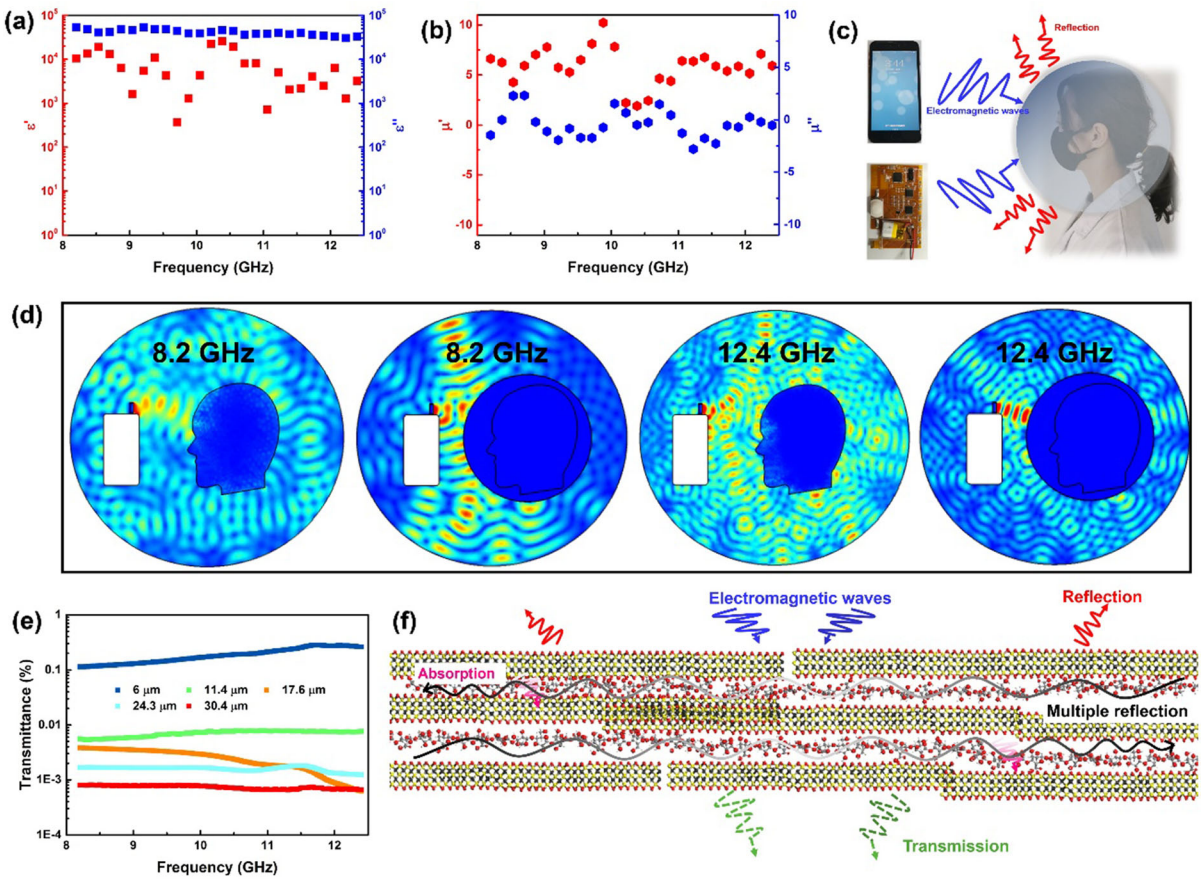

Fig. 6 **a** Permittivity and **b** permeability of the MXene/BCNF-50 composite film in the frequency range of 8.2–12.4 GHz; **c** schematic diagram of the model prototype for protecting human from electromagnetic radiation; **d** map of the electric field distribution in the microwave cavity at the frequency of 8.2 and 12.4 GHz; **e** electromagnetic wave transmittance of the MXene/BCNF-50 composite films with different thicknesses; **f** schematic illustration of the electromagnetic wave transferring across the MXene/BCNF composite film

materials (7812–30,555 dB cm^2 g^{-1}) (Shahzad et al. 2016).

Figure 6a and b show the real permittivity (ε′), imaginary permittivity (ε″), real permeability (μ′) and imaginary permeability (μ″) for MXene/BCNF-50 composite film in the frequency range of 8.2–12.4 GHz, which is used to simulate the EMI shielding efficiency to enable a visual analysis. The detailed simulation by the finite element analysis is provided in the Supporting Information, and the parameters are listed in Tables S2 to Tables S3. Figure 6c describes the schematic propagation process of the electromagnetic waves from mobile device or microchip to a human head, in which the MXene/BCNF composite material is utilized as the shielding barrier to protect human brain from electromagnetic radiation; this conceptual simulative experiment is intended to be carried out as the significant proof of concept for MXene/BCNF composite film's excellent EMI shielding performance. As shown in Fig. 6d, when the head is directly exposed to radiation, electromagnetic waves can easily pass through the skin, resulting in an increasing intensity of electric field on the side of the head close to the source, which may be harmful to human health. In contrast, when the head is completely protected by the MXene/BCNF shielding film, in the X band, the intensity distributed within both the head and air regions inside the protective film is almost invisible. Herein, transmittance (%) is calculated by EMI SE of the composite film according to Equation S9 and Equation S10, and the results are listed in Fig. 6e and Table S4. It is found

that MXene/BCNF-50 composite film with the thickness of only 11.4 μm could effectively prevent more than 99.99% electromagnetic waves from entering into the protected regions, which verifies an excellent EMI shielding performance of the composite film. To be specific, as illustrated in Fig. 6f, when the electromagnetic waves propagate at the interface between air and the conductive composite film, partial electromagnetic waves are reflected back due to the high impedance mismatch of the air-sample interface. Then the penetrating electromagnetic waves would further interact with the high-density and conductive MXene nanosheets within the composite film. Since the unique intercalated BCNF is uniformly clustered between MXene nanosheets, a largely reducing contact resistance and a frequent impedance mismatch between BCNF and MXene would induce the multiple absorption and reflection, which also results in an efficient wave absorption. On one hand, the massive and large exposed surface of in-plane oriented MXene nanosheets is the main cause of increased polarization, resulting in effective wave attenuation. Meanwhile, the rich capacitor-like interfaces formed between MXene nanosheets also play an important role in the attenuation of electromagnetic waves (He et al. 2019a; Wang et al. 2019c). Therefore, this composite film could perform an absorption-dominant EMI shielding property, promising an effective protective effect for wearers from the influence of wearable or portable electronics, such as phone, embedded microchip, and so on.

Conclusion

In this work, we report the fabrication of a robust and flexible MXene/BCNF composite film by optimizing microscopic configuration of bacterial cellulose nanofiber. By comparison with different cellulose derived MXene films, the BCNF with higher dispersion as well as larger aspect ratio is proved to be an effective reinforcing unit to construct a stable layer-by-layer self-stacking macrostructure with 2D MXene nanosheets. As a result, the optimized MXene/BCNF-50 sample could achieve both excellent tensile strength of 252.2 MPa and ideal electrical conductivity of 443.5 S cm^{-1}, respectively. Meanwhile, the sample with a thickness of only 11.4 μm presents an excellent folding endurance of more than 10,000 times, and high EMI SSE/t of 19,652 dB cm^2 g^{-1} at the frequency of 12.4 GHz. Our work provides a rational design of flexible EMI shielding film, showing great potential applications in the field of portable and wearable electronics for protecting human from electromagnetic radiation.

Acknowledgments This work was financially supported by the National Natural Science Foundation of China (52003121), the Natural Science Foundation of Jiangsu Province (BK20200501), China Postdoctoral Science Foundation (2020M671497, 2020T130300), and Priority Academic Program Development of Jiangsu Higher Education Institutions.

Author contributions XX: conceptualization, data curation, formal analysis, investigation, methodology, writing—original draft. SW: Data curation, validation. CJ: Investigation. LY: investigation. DL: investigation. YZ: software, visualization. XC: conceptualization, formal analysis, resources, visualization, writing—original draft. KW: supervision, validation, writing—review and editing. DS: supervision, validation, writing—review and editing.

References

Cao WT, Chen FF, Zhu YJ, Zhang YG, Jiang YY, Ma MG, Chen F (2018) Binary strengthening and toughening of MXene/cellulose nanofiber composite paper with nacre-inspired structure and superior electromagnetic interference shielding properties. ACS Nano 12(5):4583–4593. https://doi.org/10.1021/acsnano.8b00997

Cao MS, Cai YZ, He P, Shu JC, Cao WQ, Yuan J (2019a) 2D MXenes: electromagnetic property for microwave absorption and electromagnetic interference shielding. Chem Eng J 359:1265–1302. https://doi.org/10.1016/j.cej.2018.11.051

Cao WT, Ma C, Tan S, Ma MG, Wan PB, Chen F (2019b) Ultrathin and flexible CNTs/MXene/cellulose nanofibrils composite paper for electromagnetic interference shielding. Nano-Micro Lett 11(1):72. https://doi.org/10.1007/s40820-019-0304-y

Chen WM, Zhang DT, Yang K, Luo M, Yang P, Zhou XY (2020) Mxene ($Ti_3C_2T_x$)/cellulose nanofiber/porous carbon film as free-standing electrode for ultrathin and flexible supercapacitors. Chem Eng J. https://doi.org/10.1016/j.cej.2020.127524

Fang XY, Yu XX, Zheng HM, Jin HB, Wang L, Cao MS (2015) Temperature- and thickness-dependent electrical conductivity of few-layer graphene and graphene nanosheets. Phys Lett A 379(37):2245–2251. https://doi.org/10.1016/j.physleta.2015.06.063

Gao MH, Li J, Bao ZX, Hu MD, Nian R, Feng DX, An D, Li X, Xian M, Zhang HB (2019) A natural in situ fabrication method of functional bacterial cellulose using a microorganism. Nature Commun 10(1):437. https://doi.org/10.1038/s41467-018-07879-3

Geng L, Zhu PX, Wei YJ, Guo RH, Xiang C, Cui C, Li Y (2019) A facile approach for coating $Ti_3C_2T_x$ on cotton fabric for electromagnetic wave shielding. Cellulose 26(4):2833–2847. https://doi.org/10.1007/s10570-019-02284-5

He P, Cao MS, Shu JC, Cai YZ, Wang XX, Zhao QL, Yuan J (2019a) Atomic layer tailoring titanium carbide MXene to tune transport and polarization for utilization of electromagnetic energy beyond solar and chemical energy. ACS Appl Mater Interfaces 11(13):12535–12543. https://doi.org/10.1021/acsami.9b00593

He P, Wang XX, Cai YZ, Shu JC, Zhao QL, Yuan J, Cao MS (2019b) Tailoring $Ti_3C_2T_x$ nanosheets to tune local conductive network as an environmentally friendly material for highly efficient electromagnetic interference shielding. Nanoscale 11(13):6080–6088. https://doi.org/10.1039/C8NR10489A

Hua JC, Fei B (2019) Super-tough polyacrylamide/iota-carrageenan double-network hydrogels strengthened by bacterial cellulose microclusters. Mater Today: Proc 16:1497–1501. https://doi.org/10.1016/j.matpr.2019.05.330

Huang RK, Cao CY, Liu J, Sun DP, Song WG (2019) N-Doped carbon nanofibers derived from bacterial cellulose as an excellent metal-free catalyst for selective oxidation of arylalkanes. Chem Commun 55(13):1935–1938. https://doi.org/10.1039/C9CC00185A

Joseph N, Varghese J, Sebastian MT (2017) Graphite reinforced polyvinylidene fluoride composites an efficient and sustainable solution for electromagnetic pollution. Compos Part B-Eng 123:271–278. https://doi.org/10.1016/j.compositesb.2017.05.030

Krasteva PV, Bernal-Bayard J, Travier L, Martin FA, Kaminski PA, Karimova G, Fronzes R, Ghigo JM (2017) Insights into the structure and assembly of a bacterial cellulose secretion system. Nat Commun 8(1):2065. https://doi.org/10.1038/s41467-017-01523-2

Kumar P (2019) Ultrathin 2D nanomaterials for electromagnetic interference shielding. Adv Mater Interfaces. https://doi.org/10.1002/admi.201901454

Lee SH, Yu SG, Shahzad F, Hong JP, Kim WN, Park C, Hong SM, Koo CM (2017) Highly anisotropic Cu oblate ellipsoids incorporated polymer composites with excellent performance for broadband electromagnetic interference shielding. Compos Sci Technol 144:57–62. https://doi.org/10.1016/j.compscitech.2017.03.016

Liang CB, Song P, Ma AJ, Shi XT, Gu HB, Wang L, Qiu H, Kong J, Gu JW (2019) Highly oriented three-dimensional structures of Fe_3O_4 decorated CNTs/reduced graphene oxide foam/epoxy nanocomposites against electromagnetic pollution. Compos Sci Technol 181:107683. https://doi.org/10.1016/j.compscitech.2019.107683

Liu J, Zhang HB, Sun RH, Liu YF, Liu ZS, Zhou AG, Yu ZZ (2017) Hydrophobic, flexible, and lightweight mxene foams for high-performance electromagnetic-interference shielding. Adv Mater 29(38):1702367. https://doi.org/10.1002/adma.201702367

Liu J, Zhang HB, Xie X, Yang R, Liu ZS, Liu YF, YU, ZZ, (2018) Multifunctional, superelastic, and lightweight MXene/polyimide aerogels. Small. https://doi.org/10.1002/smll.201802479

Liu LX, Wei C, Zhang HB, Wang QW, Guan FL, Yu ZZ (2019) Flexible and multifunctional silk textiles with biomimetic leaf-like MXene/silver nanowire nanostructures for electromagnetic interference shielding, humidity monitoring, and self-derived hydrophobicity. Adv Funct Mater. https://doi.org/10.1002/adfm.201905197

Luo HL, Xiong GY, Hu D, Ren KJ, Yao FL, Zhu Y, Gao C, Wan YZ (2013) Characterization of TEMPO-oxidized bacterial cellulose scaffolds for tissue engineering applications. Mater Chem Phys 143(1):373–379. https://doi.org/10.1016/j.matchemphys.2013.09.012

Ma ZL, Kang SL, Ma JZ, Shao L, Zhang YL, Liu C, Wei AJ, Xiang XL, Wei LF, Gu JW (2020) Ultraflexible and mechanically strong double-layered aramid nanofiber–$Ti_3C_2T_x$ MXene/silver nanowire nanocomposite papers for high-performance electromagnetic interference shielding. ACS Nano 14(7):8368–8382. https://doi.org/10.1021/acsnano.0c02401

Ma C, Cao WT, Zhang W, Ma MG, Sun WM, Zhang J, Chen F (2021) Wearable, ultrathin and transparent bacterial celluloses/MXene film with Janus structure and excellent mechanical property for electromagnetic interference shielding. Chem Eng J 403:126438. https://doi.org/10.1016/j.cej.2020.126438

Malucelli LC, Matos M, Jordão C, Lomonaco D, Lacerda LG, Carvalho Filho MAS, Magalhães WLE (2019) Influence of cellulose chemical pretreatment on energy consumption and viscosity of produced cellulose nanofibers (CNF) and mechanical properties of nanopaper. Cellulose 26(3):1667–1681. https://doi.org/10.1007/s10570-018-2161-0

Nie SX, Hao NK, Zhang K, Xing CY, Wang SF (2020) Cellulose nanofibrils-based thermally conductive composites for flexible electronics: a mini review. Cellulose 27(8):4173–4187. https://doi.org/10.1007/s10570-020-03103-y

Palazzetti R, Zucchelli A (2017) Electrospun nanofibers as reinforcement for composite laminates materials—a review. Compos Struct 182(12):711–727. https://doi.org/10.1016/j.compstruct.2017.09.021

Rahman MM, Puthirath AB, Adumbumkulath A, Tsafack T, Robatjazi H, Barnes M, Wang Z, Kommandur S, Susarla S, Sajadi SM (2019) Fiber reinforced layered dielectric nanocomposite. Adv Funct Mater 29(28):1900056.1-1900056.8. https://doi.org/10.1002/adfm.201900056

Sage C, Burgio E (2018) Electromagnetic fields, pulsed radiofrequency radiation, and epigenetics: how wireless technologies may affect childhood development. Child Dev 89(1):129–136. https://doi.org/10.1111/cdev.12824

Shahzad F, Alhabeb M, Hatter CB, Anasori B, Man HS, Koo CM, Gogotsi Y (2016) Electromagnetic interference shielding with 2D transition metal carbides (MXenes). Science 353(6304):1137–1140. https://doi.org/10.1126/science.aag2421

Shen B, Zhai WT, Zheng WG (2014) Ultrathin flexible graphene film: an excellent thermal conducting material with efficient EMI shielding. Adv Funct Mater 24(28):4542–4548. https://doi.org/10.1002/adfm.201400079

Song P, Qiu H, Wang L, Liu XY, Zhang YL, Zhang JL, Kong J, Gu JW (2020) Honeycomb structural rGO-MXene/epoxy nanocomposites for superior electromagnetic interference

shielding performance. SM&T. https://doi.org/10.1016/j.susmat.2020.e00153

Tang J, Swolfs Y, Longana ML, Yu H, Wisnom MR, Lomov SV, Gorbatikh L (2019) Hybrid composites of aligned discontinuous carbon fibers and self-reinforced polypropylene under tensile loading. Compos Part A- Appl Sci Manuf 123:97–107. https://doi.org/10.1016/j.compositesa.2019.05.003

Tian WQ, Vahidmohammadi A, Reid MS, Wang Z, Hamedi MM (2019) Multifunctional nanocomposites with high strength and capacitance using 2D MXene and 1D nanocellulose. Adv Funct Mater. https://doi.org/10.1002/adma.201902977

Valekar AH, Cho KH, Lee UH, Lee JS, Yoon JW, Hwang YK, Lee SG, Cho SJ, Chang JS (2017) Shaping of porous metal–organic framework granules using mesoporous ρ-alumina as a binder. RSC Adv 7(88):55767–55777. https://doi.org/10.1039/C7RA11764G

Wan YJ, Zhu PL, Yu SH, Sun R, Wong CP, Liao WH (2018) Anticorrosive, ultralight, and flexible carbon-wrapped metallic nanowire hybrid sponges for highly efficient electromagnetic interference shielding. Small 14(27):1800534. https://doi.org/10.1002/smll.201800534

Wang S, Jiang F, Xu X, Kuang YD, Fu K, Hitz E, Hu LB (2017) Super-strong, super-stiff macrofibers with aligned, long bacterial cellulose nanofibers. Adv Mater 29(35):1702498. https://doi.org/10.1002/adma.201702498

Wang S, Li T, Chen CJ, Kong WQ, Zhu SZ, Dai JQ, Diaz AJ, Hitz E, Solares SD, Li T (2018) Transparent, anisotropic biofilm with aligned bacterial cellulose nanofibers. Adv Funct Mater 28(24):1707491. https://doi.org/10.1002/adfm.201707491

Wang L, Chen LX, Song P, Liang CB, Lu YJ, Qiu H, Zhang YL, Kong J, Gu JW (2019a) Fabrication on the annealed $Ti_3C_2T_x$ MXene/epoxy nanocomposites for electromagnetic interference shielding application. Compos Part B-Eng 171:111–118. https://doi.org/10.1016/j.compositesb.2019.04.050

Wang QW, Zhang HB, Liu J, Zhao S, Xie X, Liu LX, Yang R, Noratkar N, Yu ZZ (2019b) Multifunctional and water-resistant MXene-decorated polyester textiles with outstanding electromagnetic interference shielding and joule heating performances. Adv Funct Mater. https://doi.org/10.1002/adfm.201806819

Wang XX, Shu JC, Cao WQ, Zhang M, Yuan J, Cao MS (2019c) Eco-mimetic nanoarchitecture for green EMI shielding. Chem Eng J 369:1068–1077. https://doi.org/10.1016/j.cej.2019.03.164

Wang Y, Wang W, Qi QB, Xu N, Yu D (2020) Layer-by-layer assembly of PDMS-coated nickel ferrite/multiwalled carbon nanotubes/cotton fabrics for robust and durable electromagnetic interference shielding. Cellulose 27(5):2829–2845. https://doi.org/10.1007/s10570-019-02949-1

Weng GM, Li JY, Alhabeb M, Karpovich C, Wang H, Lipton J, Maleski K, Kong J, Shaulsky E, Elimelech M, Gogotsi Y, Taylor AD (2018) Layer-by-layer assembly of cross-functional semi-transparent MXene-carbon nanotubes composite films for next-generation electromagnetic interference shielding. Adv Funct Mater 28(44):1803360. https://doi.org/10.1002/adfm.201803360

Xie F, Jia F, Zhuo L, Lu Z (2019a) Ultrathin MXene/aramid nanofiber composite paper with excellent mechanical properties for efficient electromagnetic interference shielding. Nanoscale 11(48):23382–23391. https://doi.org/10.1039/c9nr07331k

Xie F, Jia FF, Zhuo LH, Lu ZQ, Si LM, Huang JZ, Zhang MY, Ma Q (2019b) Ultrathin MXene/aramid nanofiber composite paper with excellent mechanical properties for efficient electromagnetic interference shielding. Nanoscale. https://doi.org/10.1039/C9NR07331K

Xiong DB, Li XF, Bai ZM, Lu SG (2018) Recent advances in layered $Ti_3C_2T_x$ MXene for electrochemical energy storage. Small. https://doi.org/10.1002/smll.201703419

Yadav S, Jain CP, Sharma MM (2018) Smartphone frequency shielding with penta-bandstop FSS for security and electromagnetic health applications. IEEE T Electromagn C 61(3):887–892. https://doi.org/10.1109/TEMC.2018.2839707

Yan DX, Pang H, Li B, Vajtai R, Xu L, Ren PG, Wang JH, Li ZM (2015) Structured reduced graphene oxide/polymer composites for ultra-efficient electromagnetic interference shielding. Adv Funct Mater 25(4):559–566. https://doi.org/10.1002/adfm.201403809

Yan HQ, Chen XQ, Song HW, Li JC, Feng YH, Shi ZF, Wang XH, Lin Q (2017) Synthesis of bacterial cellulose and bacterial cellulose nanocrystals for their applications in the stabilization of olive oil pickering emulsion. Food Hydrocolloids 72:127–135. https://doi.org/10.1016/j.foodhyd.2017.05.044

Yu WC, Xu JZ, Wang ZG, Huang YF, Yin HM, Xu L, Chen YW, Yan DX, Li ZM (2018) Constructing highly oriented segregated structure towards high-strength carbon nanotube/ultrahigh-molecular-weight polyethylene composites for electromagnetic interference shielding. Compos Part A- Appl S 110:237–245. https://doi.org/10.1016/j.compositesa.2018.05.004

Zeng ZH, Jin H, Chen MJ, Li WW, Zhou LC, Zhang Z (2016) Lightweight and anisotropic porous MWCNT/WPU composites for ultrahigh performance electromagnetic interference shielding. Adv Funct Mater 26(2):303–310. https://doi.org/10.1002/adfm.201503579

Zeng ZH, Jin H, Chen MJ, Li WW, Zhou LC, Xue X, Zhang Z (2017) Microstructure design of lightweight, flexible, and high electromagnetic shielding porous multiwalled carbon nanotube/polymer composites. Small 13(34):1701388. https://doi.org/10.1002/smll.201701388

Zhang CJ, Anasori B, Seral-Ascaso A, Park SH, Mcevoy N, Shmeliov A, Duesberg GS, Coleman JN, Gogotsi Y, Nicolosi V (2017) Transparent, flexible, and conductive 2D titanium carbide (MXene) films with high volumetric capacitance. Adv Mater. https://doi.org/10.1002/adma.201702678

Zhang Q, Liang QJ, Zhang Z, Kang Z, Liao QL, Ding Y, Ma M, Gao FF, Zhao X, Zhang Y (2018) Electromagnetic shielding hybrid nanogenerator for health monitoring and protection. Adv Funct Mater 28(1):1703801. https://doi.org/10.1002/adfm.201703801

Zhang M, Wang XX, Cao WQ, Yuan J, Cao MS (2019) Electromagnetic functions of patterned 2D materials for micro–nano devices covering GHz, THz, and optical frequency.

Adv Opt Mater 7(19):1900689. https://doi.org/10.1002/adom.201900689

Zhao S, Zhang HB, Luo JQ, Wang QW, Bin S (2018) Highly electrically conductive three-dimensional $Ti_3C_2T_x$ MXene/reduced graphene oxide hybrid aerogels with excellent electromagnetic interference shielding performances. ACS Nano. https://doi.org/10.1021/acsnano.8b05739

Zhou B, Zhang Z, Li YL, Han GJ, Feng YZ, Wang B, Zhang DB, Ma JM, Liu CT (2020) Flexible, robust, and multifunctional electromagnetic interference shielding film with alternating cellulose nanofiber and MXene layers. ACS Appl Mater Interfaces 12(4):4895–4905. https://doi.org/10.1021/acsami.9b19768